

# JGR Atmospheres

## RESEARCH ARTICLE

10.1029/2019JD031261

### Key Points:

- Coupled dynamics between lake surface temperature (LST) and surface wind increases wind convergence and vertical velocity on the lee sides of the Great Lakes
- The contribution of spatial variations in LST to the increase in precipitation on the lee sides varies between 5% and 30% in three individual lake effect snow (LES) events
- The most significant impact of LST variation on winter-mean snow water equivalent (SWE) is on the lee side of Lake Huron

### Correspondence to:

P. Xue,  
pexue@mtu.edu

### Citation:

Shi, Q., & Xue, P. (2019). Impact of lake surface temperature variations on lake effect snow over the great lakes region. *Journal of Geophysical Research: Atmospheres*, 124, 12,553–12,567. <https://doi.org/10.1029/2019JD031261>

Received 3 JUL 2019

Accepted 9 NOV 2019

Accepted article online 18 NOV 2019

Published online 4 DEC 2019

## Impact of Lake Surface Temperature Variations on Lake Effect Snow Over the Great Lakes Region

Qi Shi<sup>1</sup>  and Pengfei Xue<sup>1,2</sup> 

<sup>1</sup>Great Lakes Research Center, Michigan Technological University, Houghton, MI, USA, <sup>2</sup>Department of Civil and Environmental Engineering, Michigan Technological University, Houghton, MI, USA

**Abstract** A high-resolution three-dimensional Weather Research and Forecasting (WRF) model is used to investigate the coupled impact of lake surface temperature (LST) and surface wind on the lake effect snow (LES) over the Great Lakes region. A set of twin WRF simulations, with and without resolving LST spatial variations in the model's surface boundary condition, is performed to quantify the impact of LST variation on LES. Both observations and model results reveal a positive correlation between the downwind LST gradient and surface wind convergence over the Great Lakes region. Furthermore, model simulations show that resolving the spatial variation of LST increases the surface wind convergence, correspondingly enhances local vertical motions in the atmospheric boundary layer, and creates favorable conditions for the LES formation on the lee sides of the Great Lakes. The contribution of LST spatial variations to the increase in precipitation on the lee sides of the lakes varies between 5% and 30% in individual LES events. The increase in the winter-mean snow water equivalent due to LST spatial variations is between 3% and 15%. The most significant impact of LST variation on the winter-mean snow water equivalent is on the lee side of Lake Huron.

### 1. Introduction

Due to their large size and heat capacity, the Great Lakes substantially influence the regional weather and climate by impacting the heat and water budget. The Great Lakes store heat during the summer and release heat to the ambient air during the fall and winter, which leads to cooler summertime and warmer wintertime over the Great Lakes region. Lake effect snow (LES) frequently occurs during cold seasons when a cold air mass passes over the unfrozen and relatively warm waters of the Great Lakes. The rise of the warmer, more humid, and less dense air from the lakes leads to clouds, and water vapor then freezes and deposits in the form of snow on the lee sides of the Great Lakes. LES plays a critical role in regulating the hydroclimatic system of the Great Lakes region. The average contribution of LES to the total regional winter precipitation is between 10% and 50% (Scott & Huff, 1996).

Most of the key elements that affect LES formation, such as synoptic forcing, instability, lake-air temperature difference, ice coverage, wind shear, lake orientations, and fetch have been extensively studied (Eichenlaub, 1970; Fujisaki-Manome et al., 2017; Kristovich & Laird, 1998; Niziol, 1987). In order to initiate LES, the temperature difference between the lake surface and the ambient air temperature at 850 hPa should be at least 13 °C (Villani et al., 2017). Heavy LES events are often associated with winter synoptic cyclones and cold fronts, which bring cold continental air over the warm lake waters by strong northwest winds (Notaro et al., 2013). Ice coverage also plays an essential role in LES formation (Vavrus et al., 2013; Wright et al., 2013). In general, latent heat flux (LHF) from the lakes decreases linearly with the increase in the lakes' ice coverage. Sensible heat flux (SHF) also decreases rapidly with increasing ice coverage when the ice coverage is above 70% (Gerbush et al., 2008). LES is rarely observed when the lakes' ice coverage is above 80%. Observations and modeling studies have shown a decreasing trend of ice coverage in the Great Lakes, which is favorable for the LES formation in response to climate change (Assel, 2005; Notaro et al., 2015; Zhong et al., 2016).

LES events are characterized by large spatial and temporal variations with various mesoscale and small-scale factors affecting the location and intensity of LES, which are not well understood. Several observational and modeling studies show that the land breeze induced by land-lake temperature differences plays an important role in organizing the low-level air convergence and increasing the vertical velocity (Hjelmfelt & Braham, 1983; Passarelli & Braham, 1981; Schoenberger, 1986). Laird (1999) found that mesoscale

vortices generated by lake breezes in the middle of the lake can move to the lee side of the lake and enhance the LES. Kristovich and Laird (1998) used satellite observations to find that the variation of lake-effect cloud location correlates with the variation of surface heat fluxes, which are influenced by the variation of lake surface temperature (LST) and the atmospheric stability at the boundary layer.

In addition to the mesoscale mechanisms discussed above, the coupling between water surface temperature and surface wind found in both open and coastal ocean conditions may play an important role in the LES formation. Both observational and modeling studies (Chelton et al., 2004; O'Neill et al., 2010; Schneider & Qiu, 2015; Small et al., 2008) have found that sea surface temperature (SST) modifies the surface wind in persistent SST frontal regions globally. Over the warmer side of an SST front, the surface wind speed increases with the unstable atmospheric boundary layer. High wind momentum from above descends to the surface by vertical mixing and increases the surface wind speed. On the colder side of an SST front, the surface wind speed decreases with increased boundary layer stability. The secondary circulation induced by the local pressure gradient crossing an SST front also contributes to surface wind changes. This SST-wind coupling can generate local convergences and curls of the surface wind. More specifically, studies have found the surface wind convergence positively correlates with the SST gradient along the direction of surface wind, which is termed as *downwind SST gradient* (Chelton et al., 2001; O'Neill, 2012; Schneider & Qiu, 2015). Wind divergence/convergence generated by such coupled dynamics can have profound impacts on vertical motions in the atmospheric boundary layer and resulting precipitation. During winter, water in shallow regions cools faster than water in deep areas, resulting in large LST gradients in transition zones within the Great Lakes (Ullman et al., 1998). Whether the coupling between the downwind LST gradient and the surface wind convergence exists in the Great Lakes and how it would affect the LES formation over this region remains unknown.

The focus of this study is to address two questions: (1) Does the LST and surface wind coupling exist in the Great Lakes? (2) If so, how would the coupled dynamics influence the intensity and location of LES? In this study, the Weather Research and Forecasting (WRF) model and LSTs derived from satellite observations are used to quantify the impact of the LST variation on LES. The causal relationship between the downwind LST gradient and surface wind convergence/divergence is examined, and the mechanism through which LST spatial variations affect LES is investigated.

## 2. Data and Methods

### 2.1. Data

To examine the relationship between the downwind LST gradient and surface wind divergence, LST data from the Great Lakes Surface Environmental Analysis (GLSEA) and surface wind data from the High-Resolution Rapid Refresh (HRRR) are used. The GLSEA provides daily digital maps of the Great Lakes LSTs stored as  $1,024 \times 1,024$  pixel maps with a horizontal resolution of  $\sim 1.3$  km. When ice exists, the GLSEA data also record the fractional ice coverage on each pixel, based on the data from the U.S. National Ice Center. The GLSEA LSTs are derived from Advanced Very High-Resolution Radiometer onboard polar-orbiting satellites, with an observation frequency of two to three times a day. The LST information is updated daily using the cloud-free portions of the satellite imagery. If no cloud-free imagery is available, a smooth algorithm is applied to the LST from the previous day (Schwab et al., 1992).

HRRR is a 3-km, cloud resolving, and convection-allowing atmospheric model running real time at the National Oceanic and Atmospheric Administration since September 2014. It is the first hourly updated assimilation and modeling system running operationally in the world. Radar data are assimilated into the model at 15-min intervals. HRRR uses the National Centers for Environmental Prediction (NCEP) global high-resolution SST analysis (RTG\_SST\_HR) as LST at the Great Lakes region, with a horizontal resolution of  $(1/12)^\circ$  (Benjamin et al., 2016). Recently, HRRR outputs have been designated as surface forcing for the National Oceanic and Atmospheric Administration Great Lakes Operational Forecasting System.

### 2.2. Model Configuration

The WRF model has demonstrated its success in simulating lake-air interactions and snowfalls in the Great Lakes region (Shi et al., 2010; Wright et al., 2013; Xiao et al., 2018). The Advanced Research Weather and Forecasting Model, version 4.0, is used for this study. WRF simulations are performed

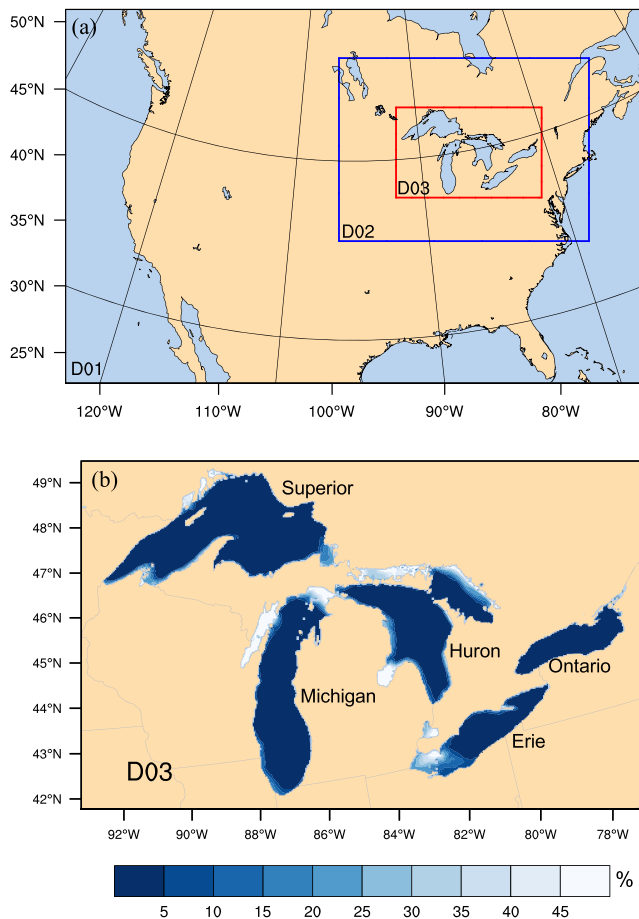


**Figure 1.** WRF model (a) three nested domains and (b) the innermost nested domain with 3-month mean ice coverage (%) in the Great Lakes for winter 2016–2017.

on three two-way nested domains (Figure 1a) with horizontal resolution of 27, 9, and 3 km, respectively. Each model domain has 69 layers in the vertical direction. The parent domain (D01) covers the continental United States and the southern part of Canada, which allows the model to simulate precursor synoptic weather systems. The innermost domain (D03) covers the entire Great Lakes region with a high spatial resolution of 3 km to resolve mesoscale processes in the lake-atmosphere boundary layer. The initial and boundary conditions for WRF simulations are from the 6-hr NCEP Operational Global Final Analyses data sets on  $0.5^\circ \times 0.5^\circ$  grids. Since the WRF model is initialized with foreign analysis, a 1-month spin-up simulation is performed from 00 UTC 1 November 2016, to allow the model and data fields to reach their balance.

The WRF model utilizes the Goddard microphysics scheme for all domains, as this scheme has been successfully applied in modeling LES events (Shi et al., 2010; Wright et al., 2013). The Kain-Fritsch cumulus scheme is employed for domains D01 and D02, while no cumulus scheme is needed for the high-resolution domain D03. Mellor-Yamada-Nakanish-Niino surface layer and boundary layer schemes are used for all domains. In the Mellor-Yamada-Nakanish-Niino scheme, the surface turbulence fluxes over water are computed by the COARE 3.0 bulk flux algorithm (Fairall et al., 2003), which is widely used in air-sea interaction applications. The Noah land surface scheme is used to simulated surface turbulent fluxes over land. The shortwave and longwave radiations are calculated using the Dudhia scheme and the Rapid Radiative Transfer Model, respectively.

### 2.3. Experiment Design

A set of twin experiments is performed. In Experiment #1 (VAR experiment), the WRF model utilizes daily GLSEA LST data as its lower surface boundary condition over the Great Lakes, which resolves spatiotemporal variations of the LST in the Great Lakes. In Experiment #2 (NON-VAR experiment), the surface water temperature in the

WRF model is updated daily using lake-mean surface temperature calculated from daily GLSEA LSTs; therefore, the impact of spatial variability of the LST in the Great Lakes on the WRF simulation is eliminated. Both simulations ran from 00 UTC 1 December 2016 to 18 UTC 28 February 2017. The SST for water points in the Atlantic Ocean and the Pacific Ocean is updated daily using the NCEP Global SST data with  $0.5^\circ$  resolution in both the VAR and NON-VAR experiments. The two simulations are identical with respect to model spatial resolution, physical parameterizations, and meteorological data used as the initial and boundary conditions.

### 3. Overview of Winter 2016–2017

The presence of extensive ice coverage on the Great Lakes has significant impact on heat and moisture fluxes (Gerbush et al., 2008). To generate LES, large ice-free lake surface is required (Wright et al., 2013). The chosen study period is the winter 2016–2017 because its annual maximum ice coverage (19.4%) is the fourth lowest since 1975. The winter-mean (December-January-February, DJF) ice coverage derived from satellite observations (Figure 1b) is less than 5% in the majority of the Great Lakes. Ice coverage greater than 40% only exists in shallow and fringe water points, such as at Green Bay, Saginaw Bay, the north shore of Georgian Bay, and the northwest shore of Lake Erie. The ice coverage located in the highly localized bays and shoreline regions should have very limited impact on lake-wide sensible and latent heat fluxes. Three 2016–2017 winter snow events were chosen for detailed case studies:

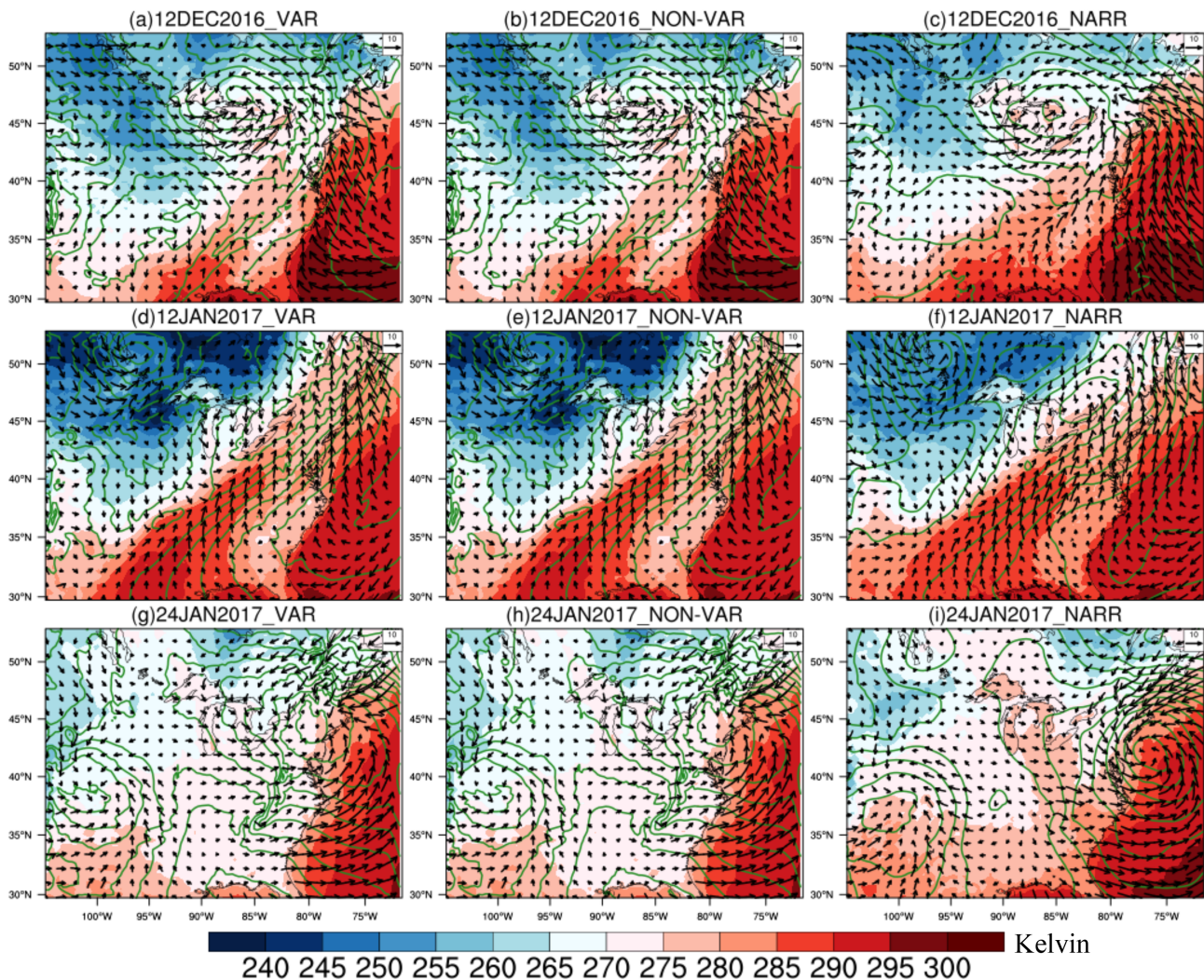


**Figure 2.** Comparison of 2-m air temperature (color shading, K), SLP (green contour, contour interval = 3 hPa), and 10-m wind (vector, m/s) among WRF VAR experiment (a, d, g), NON-VAR experiment (b, e, h), and NARR reanalysis (c, f, i) for three selected cases. For WRF simulations, surface variables from the parent domain are used.

Case 1. During 10–12 December 2016, a cross-country winter storm brought moderate to locally heavy snow to the Great Lakes region. Lake effect was reported to enhance the snowfall by 10 to 15 in. on the lee sides of lower Lake Michigan, Lake Erie, and Lake Ontario.

Case 2. During 10–12 January 2017, extreme cold arctic air associated with winter storm Jupiter traveled through the Great Lakes region and brought strong LES on the lee sides of all five lakes.

Case 3. During 24–25 January 2017, a winter storm brought widespread snowfall and strong winds (>60 mph) to the Northeastern U.S. LES was observed over the lower Great Lakes.

## 4. Results

### 4.1. Validation of WRF Simulations

To evaluate the performance of WRF in simulating the winter storms and associated LES events, the following surface variables in the three selected winter snow events described previously are assessed: sea level pressure, 10-m wind, and 2-m temperature. The North American Regional Reanalysis (NARR) with a 32-km horizontal resolution is used for comparison. NARR assimilated a large amount of observational data from radiosondes, dropsondes, pibals, aircraft, satellite, and rain gauges. For all snow events (Figure 2),

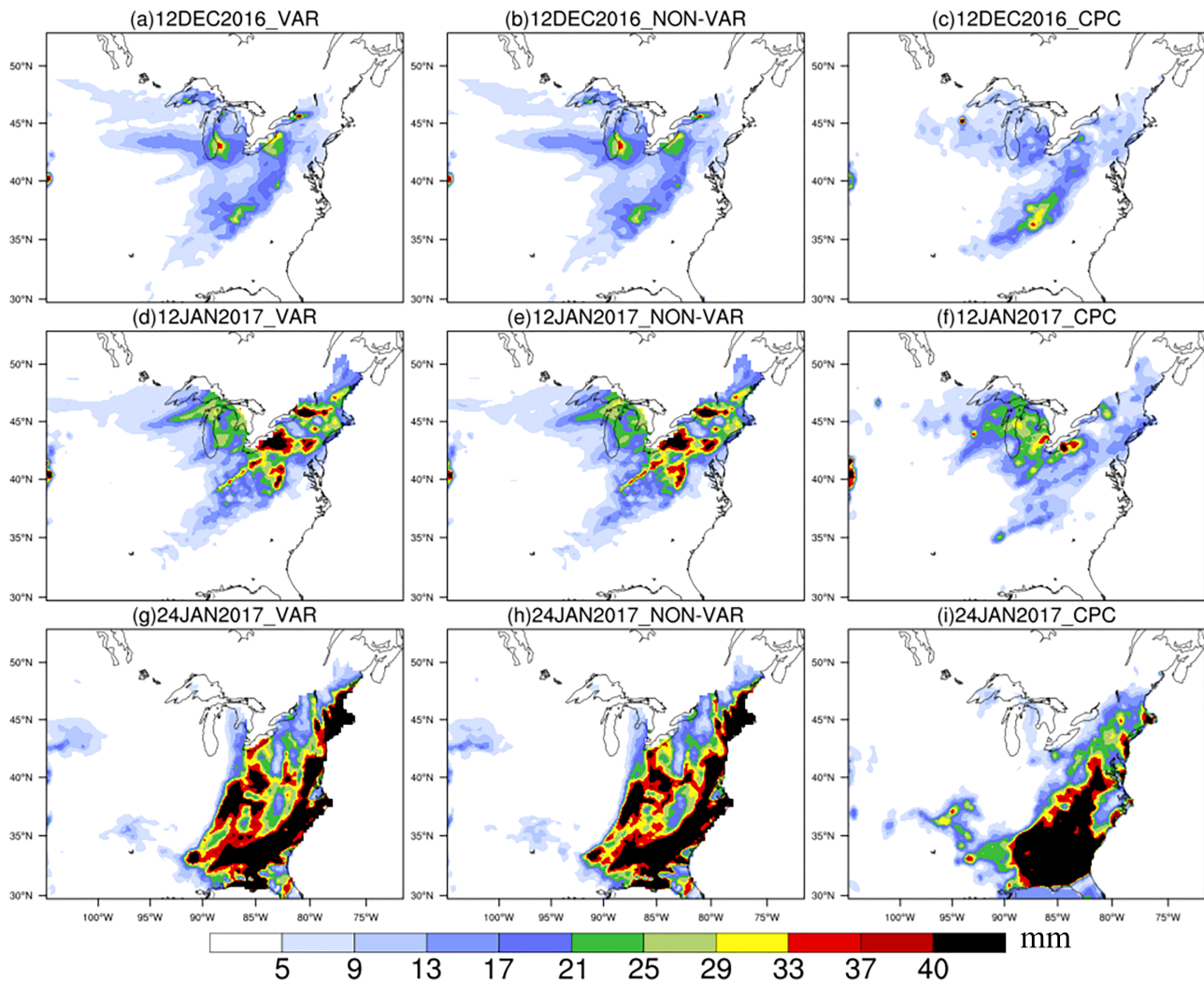


**Figure 3.** A 72-hr accumulated precipitation (mm) from WRF VAR experiment (a, d, g), NON-VAR experiment (b, e, h), and the CPC unified gauged-based analysis (c, f, i) for three selected winter storm events.

center locations of three selected surface cyclones from the WRF simulations (parent domain, 27 km) agree well with that from NARR. The intensity of sea level pressure is slightly overestimated in the WRF simulations, which was also found by Xiao et al. (2018) in their model downscaling experiments. The spatial pattern of 10-m wind and 2-m temperature from the WRF simulations also shows a good agreement with the reanalysis. By comparing the results between the VAR (Figures 2a, 2d, and 2g) and NON-VAR (Figures 2b, 2e, and 2h) experiments, we find that the LST variations do not have significant impact on the location and circulation of synoptic cyclones, which was anticipated because of much larger spatial scale of synoptic cyclones than that of the Great Lakes.

The simulated precipitation from the WRF parent domain (27 km) is verified against the 0.25° unified gauge-based analysis of daily precipitation from the Climate Prediction Center (Figure 3). The precipitation from the inner domain (3 km) is used for analyzing the impact of LST variation on LES in section 4.2. The uncertainties of precipitation during the storm events from the model and observations are both large, and the WRF model performs reasonably well in capturing large-scale patterns of the storm precipitations. To better assess the model performance skill, three statistic metrics for precipitation over the Great Lakes region are computed (Table 1). Both the VAR and NON-VAR simulations slightly overestimate the precipitation, with mean biases between 0.76 and 1.16 m/day. Results from the VAR experiment are moderately improved in terms of mean bias and root-mean-square error than that from NON-VAR experiment. The spatial pattern

**Table 1**  
Statistical Metrics of Daily Precipitation Over the Great Lakes Region From VAR and NON-VAR WRF Simulations for the Three Storms

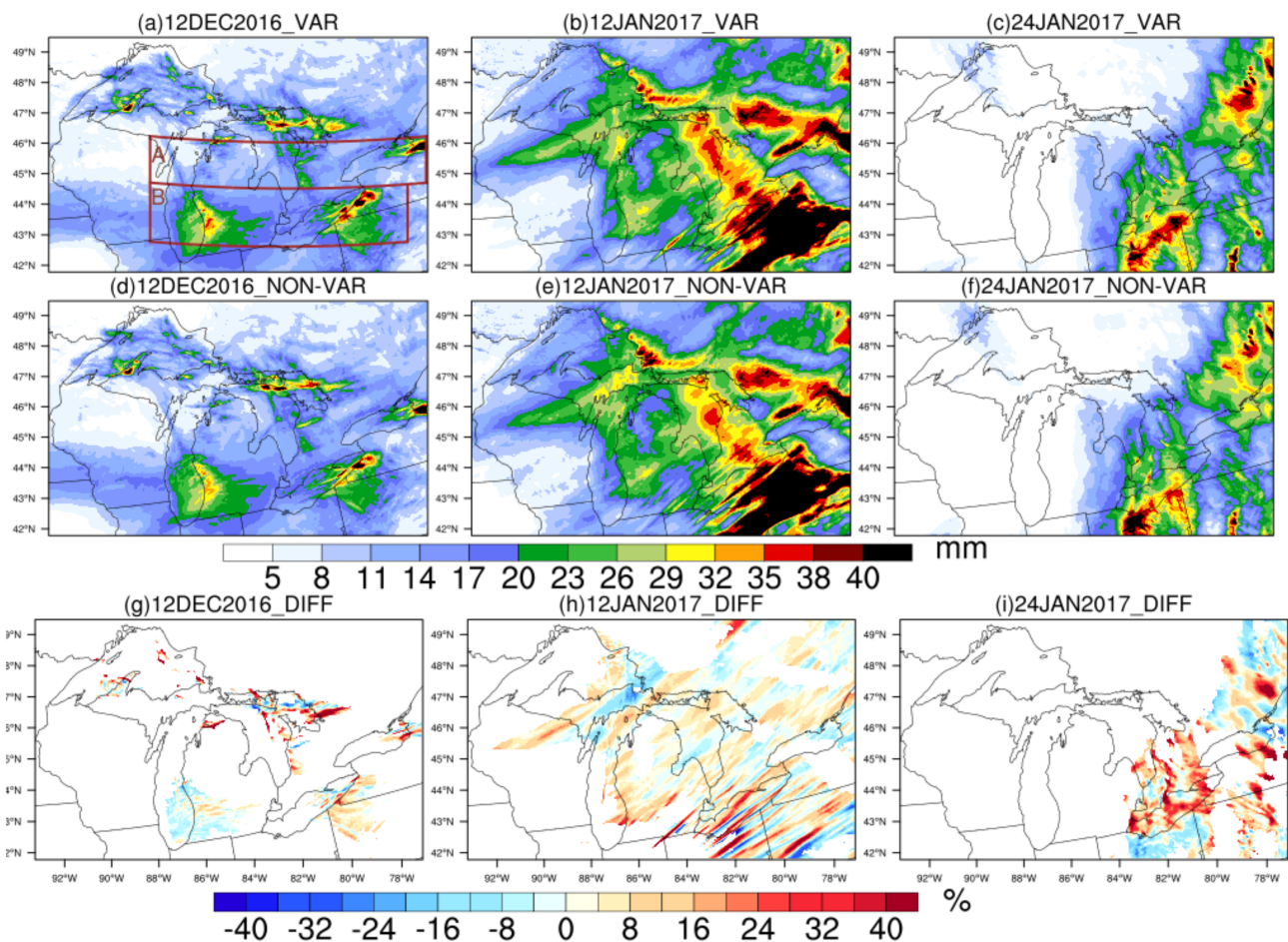
Storm	Mean bias (mm/day)		RMS error (mm/day)		Spatial pattern correlation	
	VAR	NON-VAR	VAR	NON-VAR	VAR	NON-VAR
12 Dec 2016	0.97	0.98	2.08	2.09	0.62	0.62
12 Jan 2017	0.76	0.79	3.43	3.44	0.60	0.60
24 Jan 2017	0.98	1.16	3.20	3.30	0.74	0.74

correlation ( $R$ ) between model results and observations is similar from the VAR and NON-VAR experiments. Results from both experiments successfully capture the precipitation patterns for the three snow events ( $R > 0.6$ ) over the Great Lakes region.

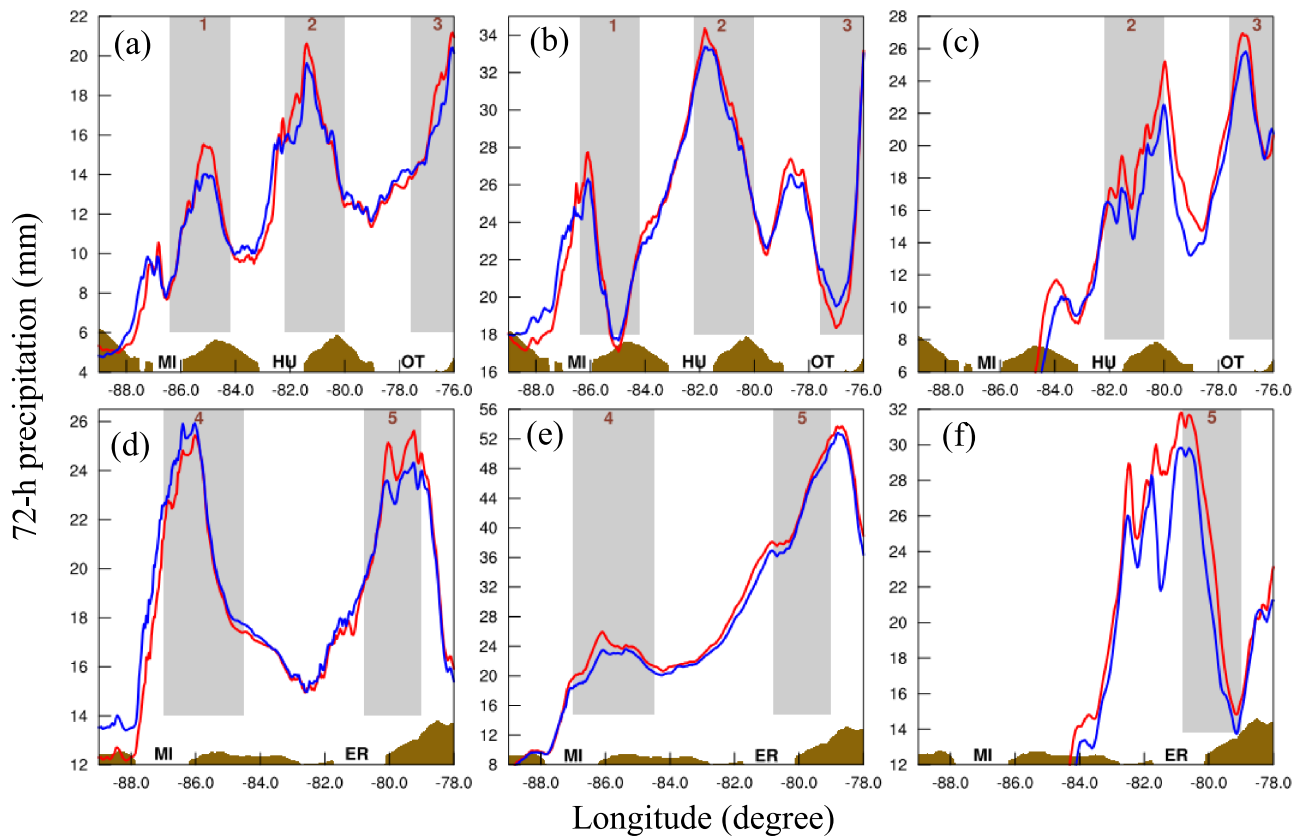
#### 4.2. Impact of LST Variation on Lake Effect Precipitation

Figure 4 compares the 72-hr accumulated precipitations from the VAR and NON-VAR experiments for three selected cases. For Case 1, LES occurs on the lee sides of lower Lake Michigan, Lake Huron, Lake Erie, and Lake Ontario (Figures 4a and 4d). The most significant difference in precipitation between the two experiments (VAR vs. NON-VAR) for Case 1 (Figure 4g) is observed in Lake Huron, where the area of strong precipitation ( $>20$  mm) expands by 59.2% over Georgian Bay, and local precipitation increases by up to 34.5% along the east shore of the bay in the VAR experiment. Significant change in precipitation in Lake Erie between the two experiments also occurs over the lee side of the lake, stretching 100 km along the southeast coast, with precipitation increasing by 8–24%. For Lake Ontario, the increase in precipitation is confined within a relatively narrow area along the east coast, within a range of 8–30%. In contrast to the other three lakes, a moderate decrease in precipitation is shown in lower Lake Michigan in the VAR experiment compared to the NON-VAR experiment.

precipitation ( $>20$  mm) expands by 59.2% over Georgian Bay, and local precipitation increases by up to 34.5% along the east shore of the bay in the VAR experiment. Significant change in precipitation in Lake Erie between the two experiments also occurs over the lee side of the lake, stretching 100 km along the southeast coast, with precipitation increasing by 8–24%. For Lake Ontario, the increase in precipitation is confined within a relatively narrow area along the east coast, within a range of 8–30%. In contrast to the other three lakes, a moderate decrease in precipitation is shown in lower Lake Michigan in the VAR experiment compared to the NON-VAR experiment.



**Figure 4.** A 72-hr accumulated precipitation (mm) from WRF VAR experiment (a–c), NON-VAR experiment (d–f), and the percentage difference (%; g–i) between VAR and NON-VAR experiments (VAR–NON-VAR) for three selected winter storm events. For the percentage difference figures, the results with 72-hr accumulated precipitation (NON-VAR) less than 20 mm are masked out.



**Figure 5.** A 72-hr accumulated precipitation (mm) averaged along box A (a–c) and box B (d–f) shown in Figure 4. The gray shading highlights the precipitation on the lee sides of Lake Michigan (1,4), Lake Huron (2), Lake Ontario (3), and Lake Erie (5). Terrain height (scaled) is indicated as brown shading at the bottom.

Strong precipitation, associated with synoptic frontal activities, occurs over the majority of Great Lakes region in Case 2, centered along the east shoreline of Lake Huron and over Lake Erie. Significant changes in precipitation between the VAR and NON-VAR experiments are also shown over the Great Lakes region (Figure 4h). The precipitation on the lee side of Lake Michigan increases by 8–24%, and the influence of LST variation extends ~100 km inland to the east of Lake Michigan (Figure 4h). The increase in precipitation on the lee side of Lake Huron is slightly less, with a magnitude of <~8%. Alternating positive and negative bands of precipitation change occur over Lake Erie as well as ~200 km inland southeast of the lake. For Lake Superior, precipitation increases by ~2% over the water and decreases by ~8% over the land (Figure 4h).

In Case 3, large 72-hr accumulated precipitations (>20 mm) occur near Lake Huron, Lake Erie, and Lake Ontario (Figures 4c and 4f). Increase in precipitation (~15–40%) in the VAR experiment is found over a large area of Lake Erie as well as over the inland east of the lake (Figure 4i). The precipitation on the lee side of Lake Huron also increases by ~16–30%.

To summarize the impact of LST variation on the location and intensity of the LES events, we calculate the meridional average of 72-hr precipitation in boxes A and B (boxes are shown in Figure 4a). Increases in meridionally averaged precipitation of 3–10% and 5–30% are observed on the lee sides of Lake Huron (Figures 5a–5c) and Lake Erie (Figures 5d–5f), respectively. Including LST, variation generally increases the precipitation on the lee side of Lake Michigan by 5–20% (Figures 5a–5c and 5e), except for the lower part of Lake Michigan in Case 1 (Figure 5d). For Lake Ontario, increases in leeward precipitation of 5% are seen in Case 1 (Figure 5a) and Case 3 (Figure 5c). In Case 2, increase in precipitation of 5% is observed over Lake Ontario and a decrease in precipitation of 15% is observed on the lee side of the lake (Figure 5b).

The impact of LST variation on the areas receiving small ( $\geq 2.5$  mm/day), medium ( $\geq 3.5$  mm/day), and large ( $\geq 4$  mm/day) amounts of winter-mean precipitation is presented in Figure 6. Winter-mean precipitation

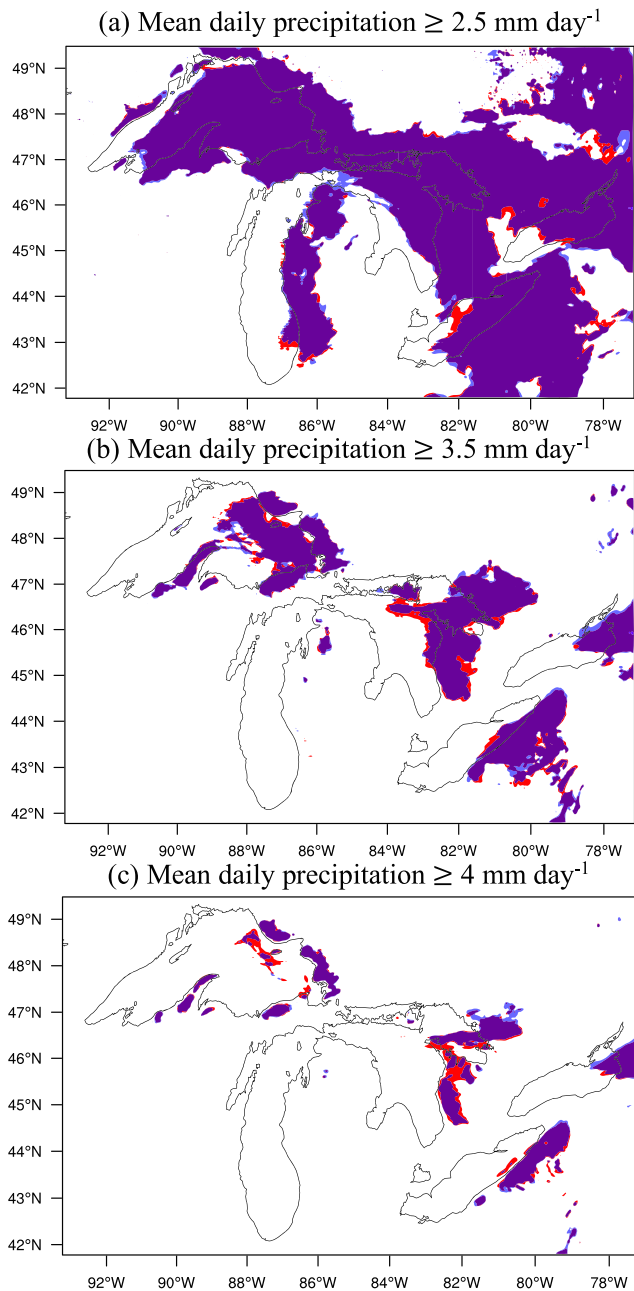


**Figure 6.** Regions of winter-mean daily precipitation greater than or equal to (a) 2.5, (b) 3.5, and (c) 4 mm/day. In each plot, the red area encloses precipitation from the VAR experiment, blue area encloses precipitation from the NON-VAR experiment, and purple areas indicate regions where red (VAR) and blue (NON-VAR) areas are overlapped.

are 0.1% and 0.7%, respectively. The percentage change in surface heat fluxes are relatively higher in Lake Ontario than in the other lakes, however still one order smaller compared to the change in the mean SWE.

## 5. Mechanisms

### 5.1. Correlation Between Downwind LST Gradient and Surface Wind Convergence

Above results quantify the impacts of LST variations on LES events; underlying mechanisms are explored in this section (section 5). Initially, the correlation between the downwind LST gradient and surface wind

greater than the selected thresholds are marked in red (VAR) and blue (NON-VAR), respectively (red and blue areas that are overlapped are shown in purple). The regions receiving winter precipitation  $\geq 2.5 \text{ mm/day}$  include the majority of the water bodies of Lake Superior, Lake Huron, Lake Erie, and Lake Ontario and a great extent of inland on the lee sides of these lakes. The only exception is Lake Michigan, over which winter-mean precipitation has not exceeded 2.5 mm/day, and precipitation  $\geq 2.5 \text{ mm/day}$  is only observed from the eastern lakeshore extending  $\sim 150 \text{ km}$  to the inland on the lee side of the lake. The regions with winter precipitation  $\geq 3.5 \text{ mm/day}$  are much smaller, and the majority is confined on the lee sides of Lake Superior, Lake Huron, Lake Erie, and Lake Ontario. A similar spatial pattern is shown for the regions with winter precipitation  $\geq 4 \text{ mm/day}$ , while the spatial extent of these regions is further reduced. The LST variation increases the leeward precipitation, most noticeably on the lee side of Lake Huron, where the land area receiving precipitation  $\geq 4 \text{ mm/day}$  has increased by 40%.

The impact of LST variation on frozen precipitation (snow) is investigated using the snow water equivalent (SWE) from WRF simulations. The area with the winter-mean SWE  $\geq 140 \text{ kg m}^{-2}$  from the VAR experiment (Figure 7a) matches well with the area receiving mean precipitation  $\geq 4 \text{ mm/day}$  (Figure 6c). Local SWE increases by  $>20\%$  on the lee sides of Lake Michigan, Lake Huron, Lake Ontario, and Lake Erie (Figure 7b) in the VAR experiment. Increases in SWE on the lee side of Lake Superior are between 4% and 8%. Decreases in SWE greater than 10% are shown on the upwind sides of Lake Michigan, Lake Huron, and Lake Erie. This is summarized in Figure 8 with the changes in the meridionally averaged SWE in boxes A and B (shown in Figure 4), which shows a clear increase in SWE on the lee sides of the Great Lakes. The largest and the second changes occur on the lee sides of Lake Huron and Lake Ontario, with the maximum increase up to  $9.34 \text{ kg/m}^2$ , and the impacted area extends up to  $\sim 150 \text{ km}$  inland.

It should be noted that surface heat fluxes are certainly important factors of LES. In the design of the VAR and NON-VAR experiments, the lake-mean LST does not change between the two experiments at any given time over the simulation duration. This ensures that surface heat fluxes do not differ significantly between the two experiments, hence allows us to isolate and identify the LES variation induced only by the spatial variation of LST. Table 2 compares changes in the mean SWE and surface heat fluxes between the two experiments. Results show that the change in surface heat flux due to LST variation is not the major contributor to the increase in snowfall on the lee sides of the Great Lakes. The winter-mean SWE increases between 6% and 12% in the VAR experiment, while increase in the lake-wide SHF and LHF due to LST variations is much smaller. In Lake Michigan and Lake Huron, the increases in SHF and LHF flux are both  $\sim 1\%$ . In Lake Erie, the increases of SHF and LHF flux

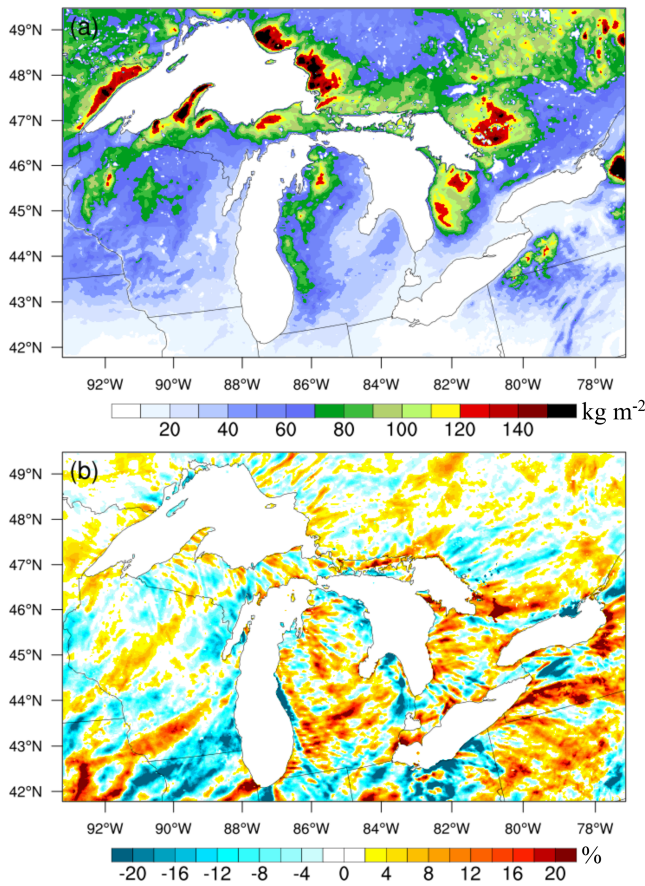


**Figure 7.** (a, b) Winter-mean SWE from the VAR experiment ( $\text{kg/m}^2$ ) and its percentage change between the VAR and NON-VAR experiments (VAR-NON-VAR, %).

and 9d, negative divergence) greater than  $3 \times 10^{-5}$  m/s is shown near the east and south shores of all five lakes. The highest pattern correlations between the downwind LST gradient and surface wind convergence are seen in Lake Michigan and Lake Huron. In the other three lakes, wind convergence zones (Figures 9b

convergence is identified. First, two independent data sets (i.e., LST from GLSEA and surface wind from HRRR) are used to identify whether a realistic correlation between the downwind LST gradient and surface wind convergence exists in the Great Lakes (Figures 9a and 9b and Figure 10, upper panels). Both data sets have similar, high spatial resolution (GLSEA LST [ $\sim 1.3$  km] and HRRR surface wind [ $\sim 3$  km]; notice HRRR includes 3 km radar assimilation) that resolves mesoscale features in the lake-atmosphere boundary layer. Second, we verify if the WRF simulations reproduce the correlation pattern and strength (Figures 9c and 9d and Figure 10, lower panels).

The *downwind LST gradient*, that is, the LST gradient along the direction of surface wind (Chelton et al., 2001; O'Neill, 2012; Schneider & Qiu, 2015), is mathematically defined as  $\nabla LST \cdot \hat{\tau}$ , where  $\nabla = \hat{i} \partial/\partial x + \hat{j} \partial/\partial y$  is the two-dimensional gradient operator with unit vectors  $\hat{i}$  and  $\hat{j}$  in the zonal and meridional directions, respectively, and  $\hat{\tau}$  is a unit vector in the direction of the surface wind. The downwind LST gradients are calculated using instantaneous wind at 3-hr interval. The mean values over winter are obtained by averaging 3-hr downwind LST gradients for DJF months.

Similar to SST and surface wind coupling at ocean SST frontal zones, positive correlation exists between the downwind LST gradient and the surface wind convergence in the Great Lakes (Figures 9 and 10). The LSTs derived from satellite observations as well as that from WRF simulations show consistent patterns of downwind LST gradients (Figures 9a and 9c) exist in coastal zones of the lakes. A strong negative downwind LST gradients zone appears near the east shore of Lake Michigan, Lake Huron, and Lake Ontario. The width of the negative LST gradient zones ( $< -1 \times 10^{-5}$  K/m) expands  $\sim 50$  km offshore from the eastern shores of Lake Michigan and Lake Huron. The downwind LST gradients over Lake Superior and Lake Erie are weaker compared to the other lakes. Wind convergence (Figures 9b

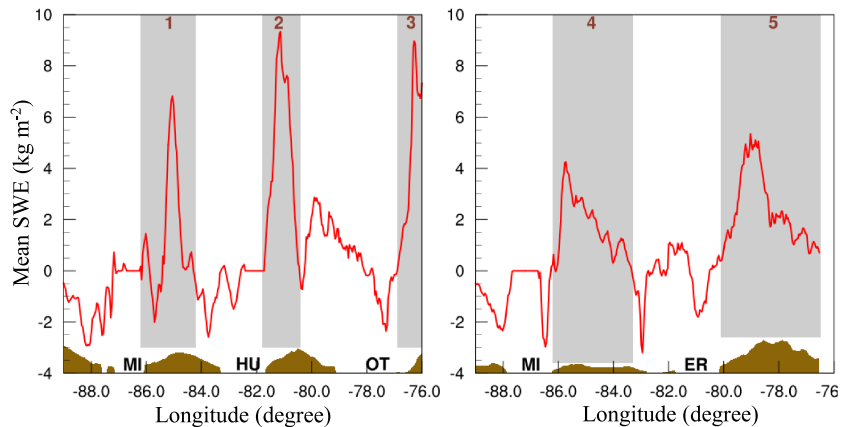


**Figure 8.** Changes in winter-mean SWE ( $\text{kg/m}^2$ , VAR-NON-VAR) averaged meridionally in boxes A and B shown in Figure 4. The gray shading highlights the SWE increases on the lee sides of Lake Michigan (1,4), Lake Huron (2), Lake Ontario (3), and Lake Erie (5). Terrain height (scaled) is indicated as brown shading at the bottom.

**Table 2**  
Percentage Change (VAR-NON-VAR) in 3-Month Mean SWE on the Lee Sides of the Great Lakes Compared With Percentage Changes in 3-Month Mean SHF and LHF for Each Lake

Lake	Mean SWE change	Total SHF change	Total LHF change
Michigan	+6.3%	+0.8%	+1.3%
Huron	+7.2%	+0.9%	+1.3%
Erie	+7.1%	+0.1%	+0.7%
Ontario	+12.6%	+2.5%	+3.3%
Superior	+3.2%	+0.3%	+0.4%

and 9d) generally cover larger areas than downwind LST gradient zones (Figures 9a and 9c). The correlation between the two can be seen more clearly in binned scatter plots (Figure 10). The increase in wind convergence corresponds linearly to the increase in the downwind LST gradient in all five lakes, that is, the stronger downwind LST gradient that exists, the stronger wind divergence/convergence coexists.

### 5.2. Coupling of Downwind LST Gradient and Surface Wind Convergence

In open oceans, the well-organized linear pattern in Figure 10 indicates the coupling between the downwind LST gradient and surface wind convergence, and the slope of the least squares fitting lines is often used to infer the sensitivity of surface wind convergence to the downwind LST gradient (Chelton et al., 2004; O'Neill et al., 2010; Putrasahan et al., 2013; Schneider & Qiu, 2015; Small et al., 2008). However, the same criteria cannot be directly applied to the Great Lakes. While a strong correlation has been identified between the downwind LST gradient and surface wind convergence, it is inappropriate to draw a conclusion on the causal relationship between the two for the Great Lakes based only on their correlation. The correlation can be caused by the sensitivity of LST to nearshore shallow bathymetry (and therefore sensitive to atmospheric cooling) and coastal wind change due to the friction contrast between overwater and overland. Therefore, the coupling of downwind LST gradient and surface wind convergence must be identified with further analysis.

Here we quantify their coupling using the *increase* in the surface wind convergence from the NON-VAR to the VAR experiments in response to the inclusion of the downwind SST gradient. This allows us to isolate

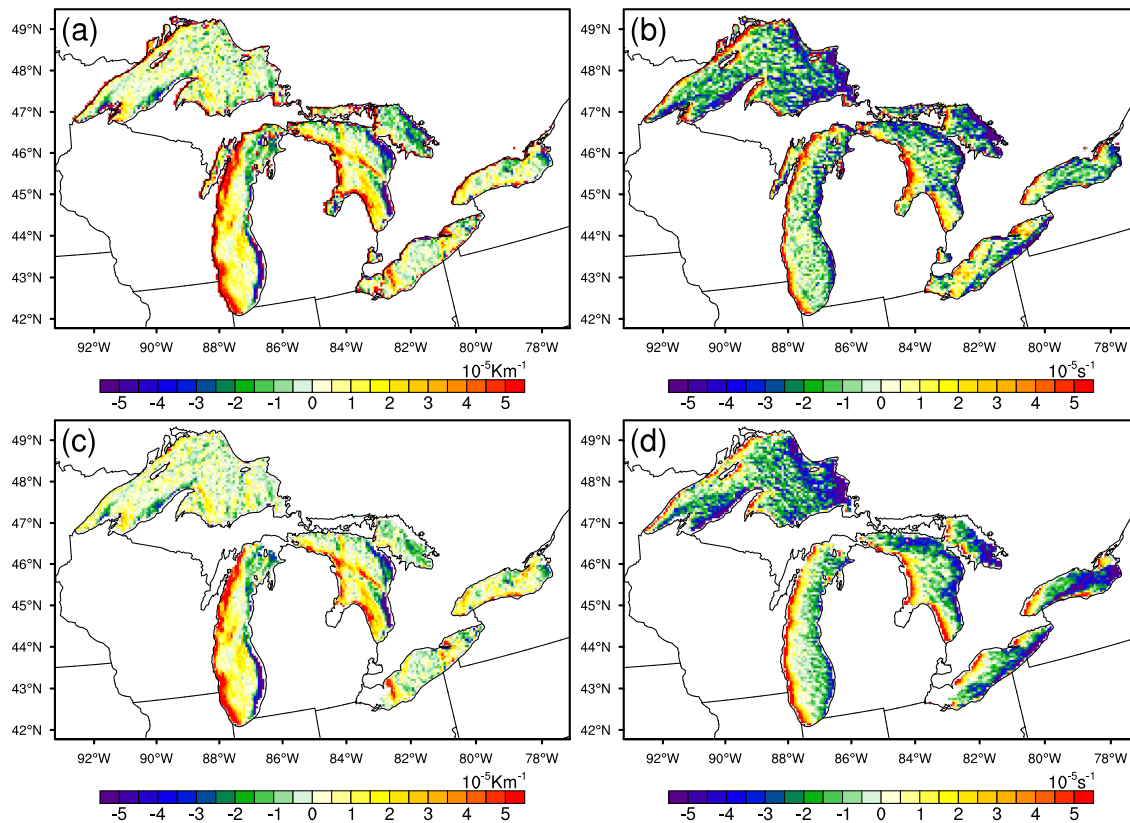


**Figure 9.** Average winter (a, c) downwind LST gradient ( $10^{-5} \text{ K/m}$ ) and (b, d) 10-m wind divergence ( $10^{-5} \text{ s}^{-1}$ ) using the LST from the GLSEA and the 10-m wind from the HRRR (top row) and the WRF VAR experiment (bottom row), respectively. For the VAR experiment (bottom row), grid points with winter-mean ice coverage greater than 20% are removed.

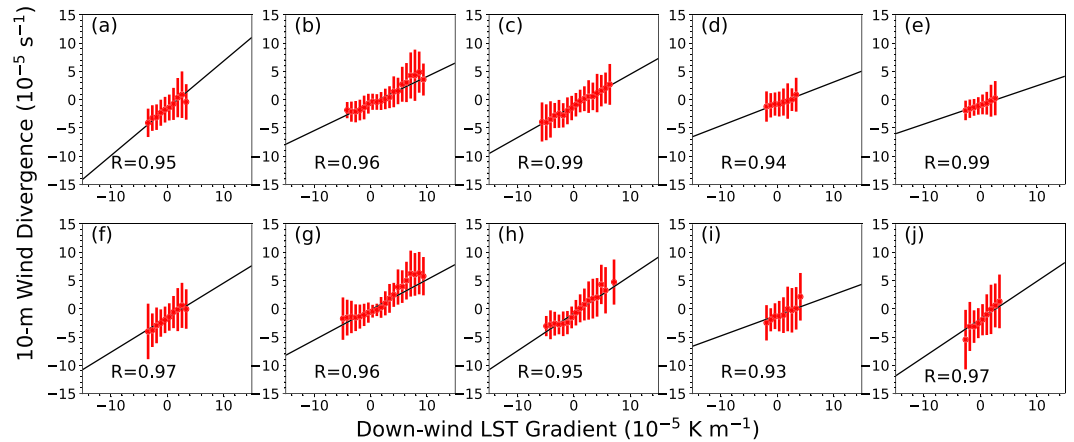


**Figure 10.** Binned scatterplots of 10-m wind divergence versus downwind LST gradient for (a, f) Lake Superior, (b, g) Lake Michigan, (c, h) Lake Huron, (d, i) Lake Erie, and (e, j) Lake Ontario. The 10-wind wind data are from HRRR in the first row and from the WRF VAR experiment in the second row. The LST data for both rows are from GLSEA (WRF VAR simulation also utilizes the GLSEA LST). Error bars represent the standard deviation within each bin. The least squares fitting of the data is indicated as blank line. The correlation coefficient between the means of the two variables in each bin is labeled at the bottom of each plot.

the surface wind convergence solely caused by downwind SST gradient from the convergence that can be induced by geometric features. Figure 11 presents the spatial patterns and statistical distributions of increase in the surface wind convergence induced by the downwind SST gradient. When LST variation is resolved in the WRF VAR experiment, surface convergence (i.e., negative divergence) increases by up to  $2.0 \times 10^{-5} \text{ m/s}^2$  over the water bodies close to the lee side of each lake from that in the NON-VAR experiment (Figure 11a), and the most significant increase occurs over the eastern Lake Huron. Moreover, the statistical pattern in Figure 11b–11f also confirms the impact of downwind SST gradient on the surface wind convergence. Results clearly show that downwind SST gradients result in increases in surface wind convergence as shown in these well-organized linear trends. The slope,  $\alpha$ , or coupling coefficient, indicates that the surface wind convergence is the most sensitive to the downwind SST gradient in Lake Huron, Lake Ontario, and Lake Erie and the least sensitive to Lake Superior. The fact that large downwind LST gradient (section 5.1) and strong LST-wind coupling (section 5.2) exist in Lake Huron supports the results in section 4, which show that the most significant impact of LST variation on LES occurs on the lee side of Lake Huron. These are direct evidences for the causal relationship between the downwind LST gradient and surface wind convergence, which reinforces the hypothesis on the dynamic linkage of the LST variation, surface wind convergence, and LES.

### 5.3. Impact of LST on Surface Wind Speed

To reveal how LST affects surface wind speed, wind speed patterns over water bodies characterized with warmer and colder LST are compared and quantified. First, winter-mean LST is computed at all model grids, denoted as  $\overline{LST}$ , where “ $\overline{\quad}$ ” indicates time averaging. Second, spatial averaging is applied to  $\overline{LST}$ , denoted as “ $\langle \overline{LST} \rangle$ ”, where “ $\langle \quad \rangle$ ” indicates spatial averaging. The perturbation of LST  $P_{LST}$  is expressed as:

$$P_{LST} = \overline{LST} - \langle \overline{LST} \rangle \quad (1)$$

Regions with a positive (negative)  $P_{LST}$  denote warmer (colder) LST relative to the winter lake mean temperature. The perturbation of surface wind speed is also calculated in the same method.

$$P_{wnd} = \overline{wnd} - \langle \overline{wnd} \rangle \quad (2)$$

Regions with a positive (negative)  $P_{wnd}$  denotes increases (decreases) in surface wind speed relative to the winter-mean wind speed.

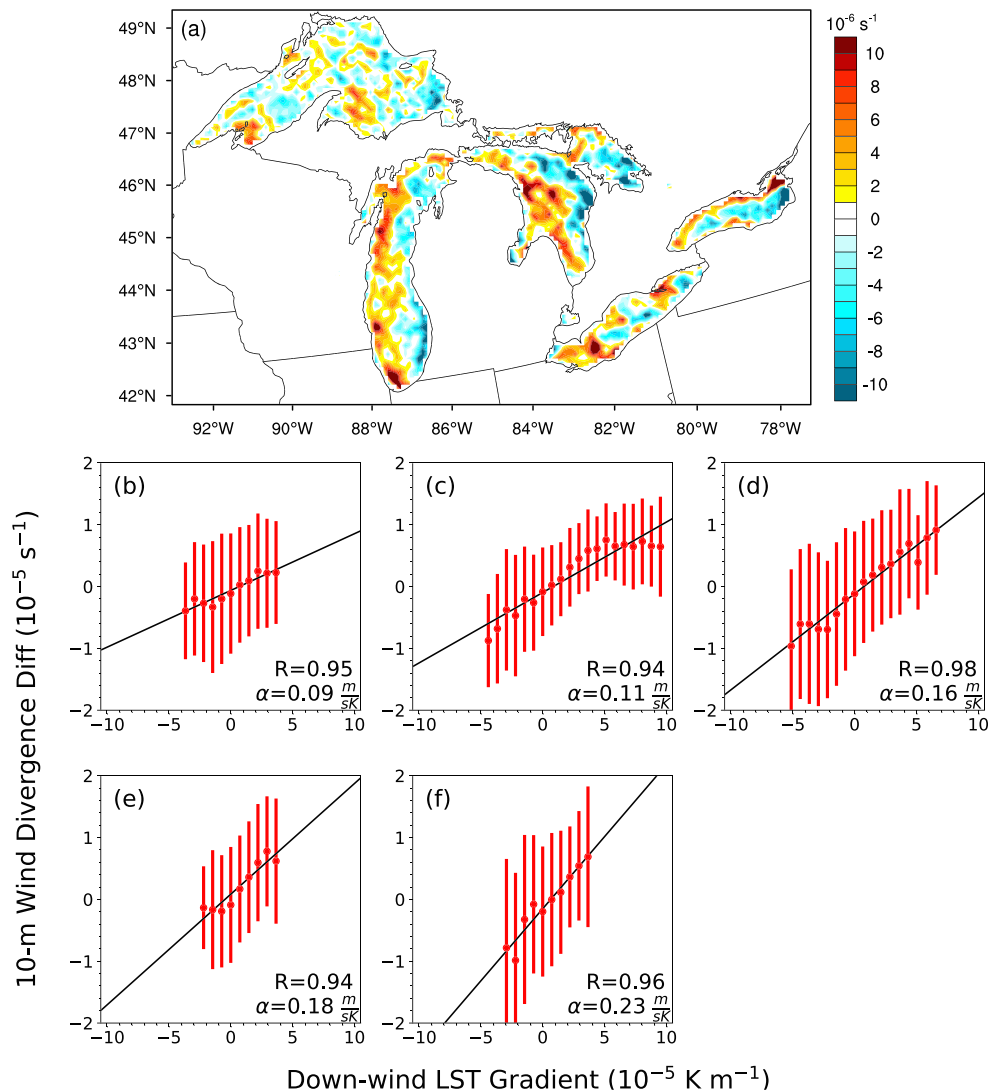


**Figure 11.** Spatial pattern distributions of the increase in the surface wind convergence induced by the downwind SST gradient. (a): spatial pattern of the change in 10-m wind divergence between VAR and NON-VAR experiment. (b–f): binned scatterplots of increase in the 10-m wind divergence (VAR–NON-VAR) versus downwind LST gradient (VAR) for (b) Lake Superior, (c) Lake Michigan, (d) Lake Huron, (e) Lake Erie, and (f) Lake Ontario. Error bars represent the standard deviation within each bin. The least squares fitting of the data is indicated as blank line. The correlation coefficient between the means of the two variables in each bin is labeled at the bottom of each plot.

The histograms of surface wind perturbations (Figure 12 show increases in surface wind speed) are, on average, over warm waters and decreases over cold waters. Therefore, the wind convergences/divergences occur over the LST fronts. Similar responses of surface wind to underlying water temperature have been shown in various oceans (Cornillon & Park, 2001; O’Neill et al., 2010; Small et al., 2008; Song et al., 2009). The modes of wind speed perturbation over warm LSTs are 0.72 m/s for Lake Huron and Lake Ontario, 0.52 m/s for Lake Superior and Lake Erie, and 0.31 m/s for Lake Michigan. The distribution of wind speed perturbation over cold LSTs generally has a larger range than over the warm waters.

#### 5.4. Impact of LST Variations on Vertical Motion

The change in the surface wind due to LST variations modifies the local convergence field and further impacts atmospheric motions in the vertical direction. The vertical motion of air in the atmospheric boundary layer enhances the transport of heat and moisture from the lake surface to the atmosphere, and its upward movement within and above the boundary layer drives water vapor condensation and cloud

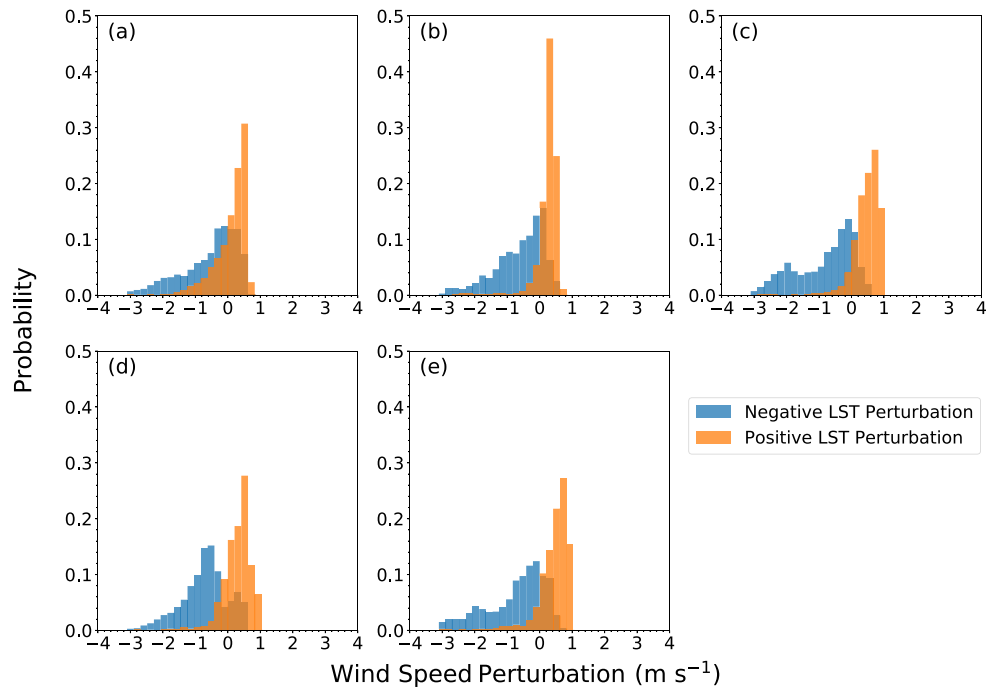


**Figure 12.** Histograms of the perturbation of surface wind speed separated between positive and negative LST perturbations from WRF VAR experiment for (a) Lake Superior, (b) Lake Michigan, (c) Lake Huron, (d) Lake Erie, and (e) Lake Ontario.

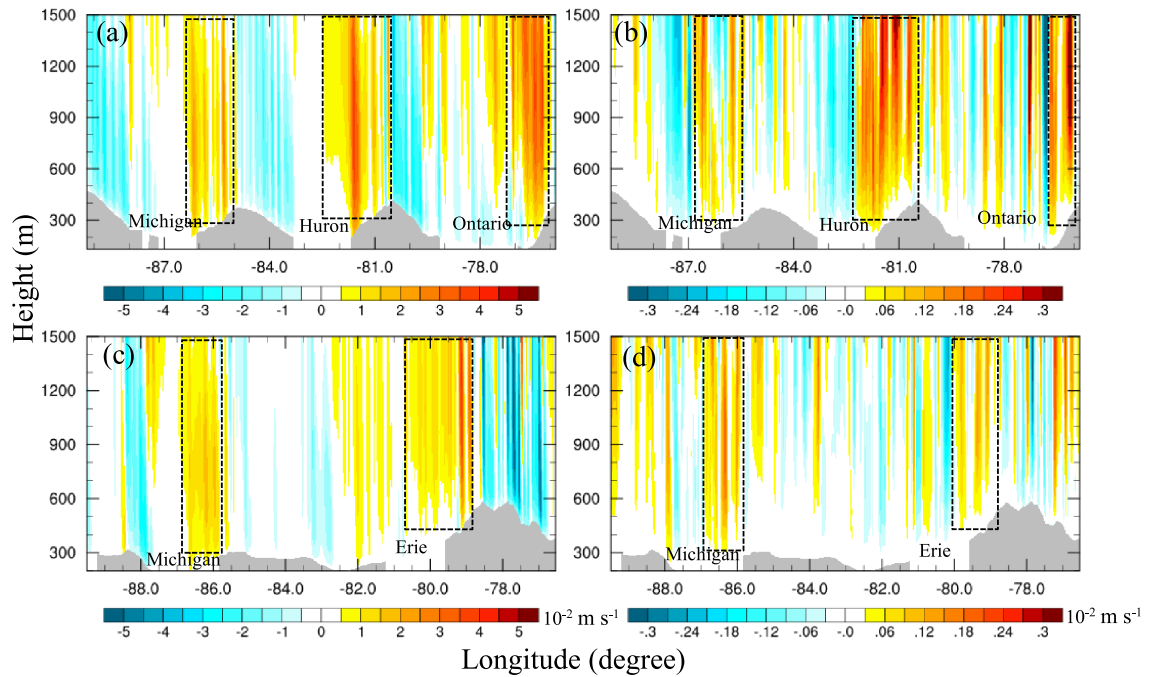


**Figure 13.** Left panels (a, c): 3-month mean vertical velocity ( $10^{-2}$  m/s) in the NON-VAR case and right panels (b, d): differences in vertical velocity ( $10^{-2}$  m/s) between the two cases (VAR-NON-VAR) averaged along box A (top) and box B (bottom) shown in Figure 4. The areas of increased vertical velocity discussed in section 5.4 are highlighted using black boxes.

formation. An increase in vertical velocity in the atmosphere helps to form thicker, deeper clouds and enhance LES. In the NON-VAR (Figures 13a and 13c) experiment, upward motions ( $>0.5 \times 10^{-2}$  m/s) are shown on the lee sides of Lakes Michigan, Lake Huron, Lake Ontario, and Lake Erie, which are related to the rising topography as well as water-land contrast in surface friction and temperature. Increases in vertical velocity due to LST variations (VAR-NON-VAR, Figures 13b and 13d) occur on the lee sides of all lakes. A wide band ( $\sim 200$  km) of vertical velocity increase, up to 15%, occurs on the lee side of Lake Huron (Figure 13b). This increase is collocated with the largest winter-mean SWE increase in Figure 8a. Strong vertical motion increase ( $>0.3 \times 10^{-2}$  m s $^{-1}$ ) also occurs on the lee side of Lake Ontario, which is collocated with the second largest increase in SWE in Figure 8a. Increase in vertical velocity by 6–10% is shown on the lee sides of Lake Michigan and Lake Erie.

## 6. Conclusions

This study provides the first detailed analysis on the coupling of the LST and surface wind and its impact on LES in the Great Lakes region using WRF simulations in combination with observational data available at the lake-atmospheric boundary layer. A set of twin WRF simulations, with and without resolving LST spatial variations in the model's surface boundary condition, is performed to identify the LST-wind coupling over the Great Lakes region, to quantify its impact on LES in this region and to explore underlying mechanisms. The major conclusions of this study include the following:

1. Including LST variations in the WRF simulation increases the precipitation in individual LES events as well as in the winter-mean precipitation on the lee sides of the Great Lakes. The contribution of spatial variations in LST to the increase in precipitation varies between 5% and 30% in three individual LES events. Increase in the winter-mean SWE induced by the spatial variation of LST is between 3% and 15%. The most significant impact of LST variation on LES is on the lee side of Lake Huron.
2. Strong correlation exists between the downwind LST gradient and surface wind convergence but only a fraction of which is due to the coupling of LST and surface wind. Using WRF twin simulations, the causal relationship between the downwind LST gradient and surface wind convergence is quantified and a mechanistic explanation on how LST variations influence the LES is provided. Wind speed generally increases (decreases) over the warm (cold) side of LST fronts in the Great Lakes, which increases the surface wind convergence over the water bodies close to the lee sides of the lakes and enhances the vertical velocity in the boundary layer in favor of LES formation. The strongest impact occurs in Lake Huron, on the leeward side of which the largest increase in the winter-mean SWE is found between the NON-VAR and VAR experiments.
3. Several factors could contribute to the coupling of LST and surface wind and its impact on LES in the Great Lakes. Fronts during the winter are formed due to strong surface cooling with cold water in shallow regions, resulting in large LST gradients in transition zones. The spatial scale of LST fronts varies among lakes, with the largest spatial scale found in Lake Huron and Lake Michigan. Lake orientation and fetch also play important roles in the LST-wind coupling. Northwest winds prevail in winter with an average wind speed between  $\sim 5$  and 10 m/s. The stronger coupling is found in Lake Ontario, Lake Huron, and Lake Erie. Both large downwind LST gradients and strong LST-wind coupling in Lake Huron make the LES on the leeward side of Lake Huron particularly sensitive to LST variations.

## References

- Assel, R. A. (2005). Classification of annual Great Lakes ice cycles: Winters of 1973–2002. *Journal of Climate*, *18*(22), 4895–4905. <https://doi.org/10.1175/JCLI3571.1>
- Benjamin, S. G., Weygandt, S. S., Brown, J. M., Hu, M., Alexander, C. R., Smirnova, T. G., et al. (2016). A North American hourly assimilation and model forecast cycle: The rapid refresh. *Monthly Weather Review*, *144*(4), 1669–1694. <https://doi.org/10.1175/MWR-D-15-0242.1>
- Chelton, D. B., Esbensen, S. K., Schlax, M. G., Thum, N., & Freilich, M. H. (2001). Observations of coupling between surface wind stress and sea surface temperature in the eastern tropical Pacific. *Journal of Climate*, *14*(7), 1479–1498. [https://doi.org/10.1175/1520-0442\(2001\)014<1479:OOCBSW>2.0.CO;2](https://doi.org/10.1175/1520-0442(2001)014<1479:OOCBSW>2.0.CO;2)
- Chelton, D. B., Schlax, M. G., Freilich, M. H., & Milliff, R. F. (2004). Satellite measurements reveal persistent small-scale features in ocean winds. *Science*, *303*(5660), 978–983. <https://doi.org/10.1126/science.1091901>
- Cornillon, P., & Park, K.-A. (2001). Warm core ring velocities inferred from NSCAT. *Geophysical Research Letters*, *28*(4), 575–578. <https://doi.org/10.1029/2000GL011487>
- Eichenlaub, V. L. (1970). Lake effect snowfall to the lee of the Great Lakes: Its role in Michigan. *Bulletin of the American Meteorological Society*, *51*(5), 403–412. [https://doi.org/10.1175/1520-0477\(1970\)051<0403:LESTTL>2.0.CO;2](https://doi.org/10.1175/1520-0477(1970)051<0403:LESTTL>2.0.CO;2)

## Acknowledgments

This is contribution 66 of the Great Lakes Research Center at Michigan Technological University. The Michigan Tech high performance computing cluster, Superior, was used in obtaining the modeling results presented in this publication. Xue's research was supported by the National Aeronautics and Space Administration, Grant 80NSSC17K0287. The NCEP Operational Global Final Analyses data set is available online (<https://rda.ucar.edu/datasets/ds083.2/>). HRRR data set is available online (<https://www.nco.ncep.noaa.gov/pmb/products/hrrr/>). GLSEA data can be obtained online ([https://coastwatch.glerl.noaa.gov/erddap/griddap/GLSEA\\_GCS.html](https://coastwatch.glerl.noaa.gov/erddap/griddap/GLSEA_GCS.html)). The NARR data set is available online (<https://www.esrl.noaa.gov/psd/data/gridded/data.narr.html>). The CPC Unified Gauge-Based Analysis is available online (<https://www.esrl.noaa.gov/psd/data/gridded/data.unified.daily.conus.html>). Due to the large size of the files, model output can be obtained by contacting the corresponding author. A copy of WRF model specifications has been uploaded from GitHub repository ([https://github.com/qishiphd/Lake\\_effect\\_snow\\_simulation](https://github.com/qishiphd/Lake_effect_snow_simulation)).

- Fairall, C. W., Bradley, E. F., Hare, J. E., Grachev, A. A., & Edson, J. B. (2003). Bulk parameterization of air-sea fluxes: Updates and verification for the COARE algorithm. *Journal of Climate*, *16*(4), 571–591.
- Fujisaki-Manome, A., Fitzpatrick, L. E., Gronewold, A. D., Anderson, E. J., Lofgren, B. M., Spence, C., et al. (2017). Turbulent heat fluxes during an extreme lake-effect snow event. *Journal of Hydrometeorology*, *18*(12), 3145–3163. <https://doi.org/10.1175/JHM-D-17-0062.1>
- Gerbush, M. R., Kristovich, D. A. R., & Laird, N. F. (2008). Mesoscale boundary layer and heat flux variations over pack ice-covered Lake Erie. *Journal of Applied Meteorology and Climatology*, *47*(2), 668–682. <https://doi.org/10.1175/2007JAMC1479.1>
- Hjelmfelt, M. R., & Braham, R. R. Jr. (1983). Numerical simulation of the airflow over Lake Michigan for a major lake-effect snow event. *Monthly Weather Review*, *111*(1), 205–219. [https://doi.org/10.1175/1520-0493\(1983\)111<0205:NSOTAO>2.0.CO;2](https://doi.org/10.1175/1520-0493(1983)111<0205:NSOTAO>2.0.CO;2)
- Laird, N. F. (1999). Observation of coexisting mesoscale lake-effect vortices over the western Great Lakes. *Monthly Weather Review*, *127*, 1137–1141.
- Kristovich, D. A., & Laird, N. F. (1998). Observations of widespread lake-effect cloudiness: Influences of lake surface temperature and upwind conditions. *Weather and Forecasting*, *13*(3), 811–821. [https://doi.org/10.1175/1520-0434\(1998\)013<0811:OOWLEC>2.0.CO;2](https://doi.org/10.1175/1520-0434(1998)013<0811:OOWLEC>2.0.CO;2)
- Niziol, T. A. (1987). Operational forecasting of lake effect snowfall in western and central New York. *Weather and Forecasting*, *2*(4), 310–321. [https://doi.org/10.1175/1520-0434\(1987\)002<0310:OFOLFS>2.0.CO;2](https://doi.org/10.1175/1520-0434(1987)002<0310:OFOLFS>2.0.CO;2)
- Notaro, M., Bennington, V., & Vavrus, S. (2015). Dynamically downscaled projections of lake-effect snow in the Great Lakes basin. *Journal of Climate*, *28*(4), 1661–1684. <https://doi.org/10.1175/JCLI-D-14-00467.1>
- Notaro, M., Zarrin, A., Vavrus, S., & Bennington, V. (2013). Simulation of heavy lake-effect snowstorms across the Great Lakes basin by RegCM4: Synoptic climatology and variability. *Monthly Weather Review*, *141*(6), 1990–2014. <https://doi.org/10.1175/MWR-D-11-00369.1>
- O'Neill, L. W., Esbensen, S. K., Thum, N., Samelson, R. M., & Chelton, D. B. (2010). Dynamical analysis of the boundary layer and surface wind responses to mesoscale SST perturbations. *Journal of Climate*, *23*(3), 559–581. <https://doi.org/10.1175/2009JCLI2662.1>
- O'Neill, L. W. (2012). Wind speed and stability effects on coupling between surface wind stress and SST observed from buoys and satellite. *Journal of Climate*, *25*(5), 1544–1569. <https://doi.org/10.1175/JCLI-D-11-00121.1>
- Passarelli, R. E., & Braham, R. R. (1981). The role of the winter land breeze in the formation of Great Lake snow storms. *Bulletin of the American Meteorological Society*, *62*(4), 482–492. [https://doi.org/10.1175/1520-0477\(1981\)062<0482:TROTWL>2.0.CO;2](https://doi.org/10.1175/1520-0477(1981)062<0482:TROTWL>2.0.CO;2)
- Putrasahan, D. A., Miller, A. J., & Seo, H. (2013). Isolating mesoscale coupled ocean-atmosphere interactions in the Kuroshio Extension region. *Dynamics of Atmospheres and Oceans*, *63*, 60–78. <https://doi.org/10.1016/j.dynatmoce.2013.04.001>
- Schneider, N., & Qiu, B. (2015). The atmospheric response to weak sea surface temperature fronts. *Journal of the Atmospheric Sciences*, *72*(9), 3356–3377. <https://doi.org/10.1175/JAS-D-14-0212.1>
- Schoenberger, L. M. (1986). Mesoscale features of the michigan land breeze using PAM II temperature data. *Weather and Forecasting*, *1*(3), 127–135. [https://doi.org/10.1175/1520-0434\(1986\)001<0127:MFOTML>2.0.CO;2](https://doi.org/10.1175/1520-0434(1986)001<0127:MFOTML>2.0.CO;2)
- Schwab, D. J., Leshkevich, G. A., & Muhr, G. C. (1992). Satellite measurements of surface water temperature in the Great Lakes: Great Lakes Coast Watch. *Journal of Great Lakes Research*, *18*(2), 247–258.
- Scott, R. W., & Huff, F. A. (1996). Impacts of the Great Lakes on regional climate conditions. *Journal of Great Lakes Research*, *22*(4), 845–863. [https://doi.org/10.1016/S0380-1330\(96\)71006-7](https://doi.org/10.1016/S0380-1330(96)71006-7)
- Shi, J. J., Tao, W. K., Matsui, T., Cifelli, R., Hou, A., Lang, S., et al. (2010). WRF simulations of the 20–22 January 2007 snow events over eastern Canada: Comparison with in situ and satellite observations. *Journal of Applied Meteorology and Climatology*, *49*(11), 2246–2266. <https://doi.org/10.1175/2010JAMC2282.1>
- Small, R. J., deSzoeke, S. P., Xie, S. P., O'Neill, L., Seo, H., Song, Q., et al. (2008). Air-sea interaction over ocean fronts and eddies. *Dynamics of Atmospheres and Oceans*, *45*(3–4), 274–319. <https://doi.org/10.1016/j.dynatmoce.2008.01.001>
- Song, Q., Chelton, D. B., Esbensen, S. K., Thum, N., & O'Neill, L. W. (2009). Coupling between sea surface temperature and low-level winds in mesoscale numerical models. *Journal of Climate*, *22*(1), 146–164. <https://doi.org/10.1175/2008JCLI2488.1>
- Ullman, D., Brown, J., Cornillon, P., & Mavor, T. (1998). Surface temperature fronts in the Great Lakes. *Journal of Great Lakes Research*, *24*(4), 753–775.
- Vavrus, S., Notaro, M., & Zarrin, A. (2013). The role of ice cover in heavy lake-effect snowstorms over the Great Lakes Basin as simulated by RegCM4. *Monthly Weather Review*, *141*(1), 148–165. <https://doi.org/10.1175/MWR-D-12-00107.1>
- Villani, J. P., Jurewicz, M. L. Sr., & Reinhold, K. (2017). Forecasting the inland extent of lake effect snow bands downwind of Lake Ontario. *Journal of Operational Meteorology*, *05*(05), 53–70. <https://doi.org/10.15191/nwajom.2017.0505>
- Wright, D. M., Posselt, D. J., & Steiner, A. L. (2013). Sensitivity of lake-effect snowfall to lake ice cover and temperature in the Great Lakes region. *Monthly Weather Review*, *141*(2), 670–689. <https://doi.org/10.1175/MWR-D-12-00038.1>
- Xiao, C., Lofgren, B. M., & Wang, J. (2018). WRF-based assessment of the Great Lakes' impact on cold season synoptic cyclones. *Atmospheric Research*, *214*, 189–203. <https://doi.org/10.1016/j.atmosres.2018.07.020>
- Zhong, Y., Notaro, M., Vavrus, S. J., & Foster, M. J. (2016). Recent accelerated warming of the Laurentian Great Lakes: Physical drivers. *Limnology and Oceanography*, *61*(5), 1762–1786. <https://doi.org/10.1002/lno.10331>